



CHORUS

This is the accepted manuscript made available via CHORUS. The article has been published as:

Graphene as an alignment agent, an electrode, and a source of surface chirality in a smectic-A liquid crystal

Rajratan Basu

Phys. Rev. E **103**, 022710 — Published 25 February 2021

DOI: [10.1103/PhysRevE.103.022710](https://doi.org/10.1103/PhysRevE.103.022710)

Graphene as an alignment-agent, an electrode, and a source of surface chirality in a smectic-*A* liquid crystal

Rajratan Basu*

Department of Physics, Soft Matter and Nanomaterials Laboratory, The United States Naval Academy, Annapolis, MD 21402, USA.

A liquid crystal (LC) cell was fabricated by putting together a monolayer graphene-coated glass substrate on one side, and a rubbed planar-aligning polyimide layer on an indium tin oxide (ITO) coated glass substrate on the other side. The monolayer graphene film served as the planar-alignment agent as well as the transparent electrode on one side of the cell. The cell was filled with an *achiral* LC alkoxyphenylbenzoate (9004). The presence of the graphene film on one substrate resulted in an induced chiral signature in the otherwise achiral LC 9004. The induced chirality was probed utilizing the electroclinic effect (a polar tilt of the LC director perpendicular to, and linear in, an applied electric field) in the smectic-*A* phase. The electroclinic effect showed significant pretransitional behavior on approaching the smectic-*A*—smectic-*C* transition temperature from above. The electroclinic effect revealed a low-frequency relaxation process indicating that the chirality was induced on the LC molecules at the graphene interface and did not propagate into the bulk. A soft shear mode can break the symmetry of the hexagonal lattice of graphene on a substrate, and consequently, graphene possesses strain chirality. The non-covalent π - π interaction between the LC and the strained graphene induces molecular conformational deracemization in the LC at the graphene interface, and the LC exhibits surface-induced chirality.

* Corresponding author: basu@usna.edu

I. INTRODUCTION

In liquid crystal (LC) science, chirality is one of the most important and exciting topics to explore. Chiral induction-based phenomena in LCs have been known for some time. In the LCs, the induction of chirality in the molecules breaks the mirror symmetry. Chirality can be induced in otherwise achiral LCs employing various methods. For example, chirality can be induced in LCs by doping nanomaterials, such as carbon-nanotubes [1,2,3,4,5] and chiral periodic mesoporous organosilicas [6,7]. A macroscopic torsional strain from a twist-cell can induce chirality in LCs [8,9,10]. Various chiral patterns on the alignment substrates in the LC cell can also transmit chirality in LCs [11,12,13]—which is the essence of *surface-induced chirality* in LCs.

This surface-induced chirality in achiral LCs, utilizing different techniques (*e.g.*, by scribing a chiral pattern into a spatially isotropic substrate [11] and using a highly oriented pyrolytic graphite substrate [14]), is an important avenue in fundamental research to understand the surface chirality transmission mechanism [12,13] into the LC. In this area, we are reporting that when a monolayer graphene film on a glass substrate is used as an alignment agent in an LC cell, a surface chirality transmission phenomenon is observed in the Sm-*A* phase—which is probed by the frequency-dependent electroclinic effect.

Garoff and Meyer first observed the electroclinic effect (ECE) in a chiral smectic-*A* (Sm-*A*) phase [15]. This ECE is an induced polar tilt angle θ of the LC director (\hat{n}) perpendicular to, and linear in, an electric field E that is applied parallel to the smectic layers. The ECE coefficient, $e_c = \frac{d\theta}{dE}$, increases, and eventually diverges on cooling toward the chiral smectic-*C**

(Sm- C^*) phase. An ECE requires the reduced C_2 symmetry of the lower temperature Sm- C^* phase. When the system is achiral, the ECE is not observed

Graphene is a crystalline allotrope of carbon where the carbon atoms are densely packed in an sp^2 -bonded atomic-scale hexagonal pattern in two-dimension (2D). In the hexagonal graphene lattice, the C—C bond length is 1.42 Å. In a hexagonal benzene ring, the C—C bond length is 1.40 Å. The hexagon in the graphene lattice and the hexagon of the benzene ring have almost the same size. Therefore, the LC molecules coherently align on the 2D graphene surface [16,17,18] (and other graphene-like surfaces [19,20,21,22]) due to epitaxial interactions between the benzene rings of the LC molecules and the hexagonal lattice of graphene, employing the π – π electron stacking interaction with the binding energy ranging from 0.74 to 0.88 eV/molecule [23]. We have previously shown that graphene can serve as the planar-alignment agent for a nematic LC in a uniform planar LC cell due to this graphene—LC interaction [24,25,26].

When graphene is deposited on a substrate or one graphene layer is on top of another graphene layer, a soft shear mode is generated at the interface—which results in a strain on the graphene surface [27]. It has been experimentally demonstrated that the presence of this strain breaks the hexagonal lattice symmetry in graphene, and consequently, graphene exhibits circular dichroism [27]—which is the indication of the presence of chirality at the graphene surface. We have previously demonstrated that when a small quantity of graphene flakes are dispersed in an achiral LC in colloidal form, the strain chirality of graphene can be transmitted into the LC molecules; and the LC exhibits two types of bulk chiral signatures: a bulk ECE in the Sm- A phase and a macroscopic helical twist of the LC director in the nematic phase [28,29]. Other hexagonal 2D materials are also found to exhibit the chirality transmission phenomenon. For example, it was experimentally shown that an achiral Sm- C LC on the MoS₂ surface (which has

a similar hexagonal structure like graphene) manifests the macroscopic sawtooth-shaped streaks—which indicates that the MoS₂'s surface chirality is transmitted into the LC [30].

II. EXPERIMENTS, RESULTS, AND DISCUSSION

Now we ask the question: what happens in terms of the chirality transmission phenomenon if graphene is present in the form of a monolayer film on a substrate (and not in the form of flakes as colloidal dispersion)? In this present work, we have designed a planar LC cell by placing together a monolayer graphene-coated glass slide, and a planar-aligning rubbed polyimide (PI) layer on an indium tin oxide (ITO) coated glass slide. We then show that an LC in the Sm-*A* in this hybrid cell exhibits a strongly frequency-dependent ECE signal, which suggests that it is predominantly a surface effect where the chirality is transmitted into the LC molecules near the LC/graphene interface and does not propagate well into the bulk.

A. Fabrication of the graphene-PI hybrid LC cell

We have employed the standard polymethyl-methacrylate (PMMA) assisted wet transfer method [31,32] to transfer the commercially obtained (*Graphene Supermarket, Inc.*) large-scale monolayer graphene film [33] from a copper foil onto a glass substrate. The sheet resistance of the graphene film on the glass was found to be $\sim 660 \Omega/\square$. The monolayer graphene-coated glass slide was placed together with a unidirectionally rubbed planar-aligning PI (KPI-300B) substrate on an ITO coated glass slide (from *Instec, Inc.*) to make a graphene-PI cell with an average cell-gap of $9.3 \mu\text{m}$. The monolayer graphene film and the PI substrate faced each other in the cell.

On the graphene side of the cell, the graphene film serves as the planar-alignment layer and the transparent electrode, simultaneously. On the PI side, the ITO serves as the transparent electrode. The cell was filled with the LC alkoxyphenylbenzoate (9004) in the isotropic phase

by capillary action. And then, the cell was then brought in the Sm-*A* phase. The chemical structure and the cooling phase sequence of LC 9004 are given in Fig. 1(a). The graphene-PI LC cell is schematically illustrated in Fig. 1(b). Figure 1(c) shows the picture of this hybrid cell. The monolayer graphene on one side and the rubbed PI on the other side impose homogenous alignment on the LC. The mechanism of achieving a uniform planar alignment of the LC in the graphene-PI cell is discussed elsewhere [25,26]. The alignment of the Sm-*A* phase in the graphene-PI cell was studied by rotating the cell under a crossed-polarized microscope. The micrographs in Figs. 1(d) and 1(e) show the orientation of \hat{n} at 45° (uniformly bright) and 0° (uniformly dark), respectively, with respect to the polarizer. These results suggest that the Sm-*A* phase obtained good alignment in the LC. A standard commercial uniform planar cell (rubbed PI on both sides) from *Instec, Inc.*, with a cell-gap of $10\ \mu\text{m}$, was also filled with 9004 for a comparative study.

B. Electroclinic measurements

For the ECE measurement, we have used the classical “electroclinic geometry” [34], where the optical setup had a 5-mW He-Ne laser beam ($\lambda = 633\ \text{nm}$) that passed through a polarizer, the cell, a crossed analyzer and into a photodetector (PDA100A, Thor Labs). The beam was polarized at an angle of 22.5° with respect to the cell’s rubbing direction. For the graphene-PI LC cell, the graphene side faced the detector. The output of the detector was fed into both a lock-in amplifier (Stanford Research Systems SR830 DSP) and to a dc voltmeter (Keithley 2002). The lock-in amplifier was referenced to the driving frequency f of the applied electric field from a signal generator (Stanford Research Systems SR345). This setup allowed us to measure the ac intensity I_{ac} at frequency f from the lock-in amplifier and the dc intensity I_{dc} from the dc voltmeter. Note that when the voltage was applied across the graphene-PI cell, the

electric field was generated between the graphene electrode and the ITO electrode. The setup and data acquisition were computer-controlled using LabVIEW[®] software. The field-induced effective tilt angle θ was obtained from the measured ac and dc intensities using the formula $\theta = \frac{I_{ac}}{4 I_{dc}}$. This is a standard technique to measure θ vs. E (f) for the ECE in chiral LCs [7,35,36,37]. In mean-field theory, the field-induced tilt angle $\theta = \frac{kc^*}{\alpha(T-T_{AC^*})}E$ [38], where T_{AC^*} is the Sm-*A* to Sm-*C** transition temperature, k is the susceptibility, c^* is the chiral coupling coefficient (which vanishes in the absence of chirality), and α is the non-chiral coefficient.

Figure 2 shows the effective tilt angle θ as a function of the rms applied field E at $f = 100$ Hz for 9004 in the (a) standard commercial uniform planar cell and (b) graphene-PI cell. The achiral LC 9004 in the standard commercial uniform planar cell does not show any ECE signal in the Sm-*A* phase, verifying the absence of molecular chirality associated with pure 9004. On the other hand, 9004 in the graphene-PI cell exhibits a linear increase in effective tilt angle θ with increasing E . It is important to note here that we were not able to increase E above 2.5 V/ μ m due to the hydrodynamic instabilities in the LC. The linear ECE ($E \leq 2.5$ V/ μ m) grows on cooling toward T_{AC^*} , demonstrating the presence of induced chirality in the Sm-*A* phase. We also examined the temperature behavior of the ECE of the mixture above T_{AC^*} ($= 62^\circ$ C). The electroclinic coefficient, $e_c = \frac{d\theta}{dE} = \frac{kc^*}{\alpha(T-T_{AC^*})}$ was found to increase on cooling, with an apparent divergence at T_{AC^*} , as shown in Fig. 3(a). Figure 3(b) shows e_c^{-1} vs. T , observing an approximately linear variation with T close to T_{AC^*} . This is consistent with mean-field behavior and with previous results on inherently chiral LCs [34,35]. Notably, e_c diverges at T_{AC^*} , indicating that the observed effect indeed corresponds to the coupling between E and the graphene-induced chiral LC domains, rather than a direct electric field – graphene film coupling.

It is also important to point out that the magnitude of e_c observed in this experiment is a few orders of magnitude smaller than that of the inherently chiral LCs [15,34], indicating weak chirality transfer from the strained graphene surface.

C. Discussion

LC 9004 is configurationally achiral LC. However, 9004 can adopt a chiral conformation in the ground state by rotating left or right about the Ph–O bond [6]. This rotational barrier for 9004 is quite low ~ 0.4 kcal mol⁻¹ [6]. An equal probability distribution between left and right twist makes them dynamically racemic. As discussed earlier, the LC director aligns along the graphene surface [16], employing the π – π electron stacking between the honeycomb structure of graphene and benzene rings of the LC. Note that the energy associated with this π – π electron stacking interaction (~ 0.88 eV ≈ 85 kcal mol⁻¹) [23] is three orders of magnitude higher than the rotational barrier energy for 9004.

When graphene is deposited on a substrate, it can naturally develop strong surface corrugations, and this buckling can create regions of high and low strain [39]. As discussed earlier, the presence of this strain breaks the hexagonal lattice symmetry in graphene, which leads to a circular dichroism signal from graphene [27]. This is the indication of the presence of structural chirality at the graphene surface. In our experiment, graphene is deposited on a glass substrate using the PMMA assisted wet transfer method. During this transfer process, the graphene layer experiences lateral forces on the glass substrate. Consequently, a shear stress is developed on the graphene layer along the average direction of these lateral forces. This shear stress results in a shear strain on the graphene surface, breaking the mirror symmetry preferentially into either right-handed or left-handed domains depending on the direction of the

shear stress. Overall, this shear strain is uniform on the surface. So, when the graphene surface gains strain-chirality due to this shear mode, the 9004 LC molecules, attached to the graphene surface, adopt that surface chirality by shifting its equilibrium between left- and right-handed chiral conformers by rotation about the Ph–O bond to compensate the elastic energy cost, and still maintaining the π – π electron stacking interaction between the LC and graphene. This happens because π – π electron stacking interaction is much stronger than the rotational barrier energy for 9004. This process produces a statistically higher population of chiral conformers of one handedness, breaking the symmetry between right-and left-handed molecular conformations—which is also called deracemization. The strained graphene surface and the twist on 9004 molecules about the Ph–O bond are schematically shown in Fig. 1(f). We observed the electroclinic effect in LC 9004 due to this symmetry breaking in the LC through deracemization.

We have repeated this ECE measurement at four different positions on the cell (*i.e.*, the laser beam was moved to four different spots on the cell), and the ECE signals were reproducible within 5 to 8% deviations. This ensures that the ECE signals are indeed from the induced-chiral LC and not from any random defects in the cell.

The *bulk* ECE is intrinsically very fast [38]. In fact, the bulk ECE is the fastest of the useful electro-optic effects in liquid crystals, with a speed allowing MHz switching rates in repetitive operation [38,40,41,42]. However, when the chirality is present only near the LC/substrate interface, the director tilt θ does not elastically propagate well into the bulk LC and is localized near the LC/substrate interface. At high frequencies, the director tilt θ (near the LC/substrate interface) cannot follow the ac field adiabatically because of the strong LC/substrate interaction. Thus, the ECE shows a strong frequency-dependent behavior (*i.e.*, a

relaxation process) and dies off well below the MHz regime [7,8,43]. This is the hallmark of a *surface* ECE. Therefore, chiral surface-induced ECE studies are conducted at low frequencies ($f \leq 100$ Hz) [11,12,13] to ensure that the director tilt would follow the ac field adiabatically. At higher frequencies, this optical adiabatic-following drops dramatically—which results in a significant decrease in the chiral surface-induced ECE.

We have studied the ECE as a function of frequency for the graphene-PI cell. Using the same electro-optic setup, the ECE was measured at a constant applied field $E = 2$ V/ μm , with varying the frequency from $1 - 10^4$ Hz at $T = 63$ °C (right above $T_{AC^*} = 62$ ° C). Figure 4 shows e_c as a function of frequency f —which exhibits a relaxation process. **The ECE decreases significantly above $f \approx 10^3$ Hz.** This quick drop suggests that only a few layers of Sm-*A* LC on the strained graphene surface gain chirality, which does not elastically propagate into the bulk. This also indicates that the electroclinic director tilt in the Sm-*A* phase does not have much optical adiabatic following at higher frequencies.

In our previous work [28], we showed that the presence of graphene flakes in the LC in colloidal form induces *bulk* chirality, and the ECE remained unchanged in the frequency range from 1 Hz to 10^4 Hz. This is because the induced chiral LC domains surrounding the graphene flakes were uniformly present throughout the bulk LC and the entire LC behaved as a chiral LC. Our present work is a limiting case where one can imagine the graphene flakes are stitched together to make a monolayer graphene film, which is now attached to a substrate and induces surface ECE. In both these cases, the induced chirality is very small but measurable by the ECE.

III. CONCLUSION

To summarize, we have first demonstrated that replacing a rubbed PI with a monolayer graphene film in an LC cell still maintains the homogenous alignment for the Sm-*A* phase. Here, graphene is simultaneously utilized as the planar-alignment agent and the electrode at one side of the cell. The strain on graphene, due to natural corrugations, induces chirality in the otherwise achiral LC 9004. The chirality was probed utilizing the ECE in the Sm-*A* phase. The ECE shows an apparent pretransitional behavior on approaching the Sm-*C* phase from above. The induced chirality is present predominantly at the graphene/LC interface and does not disseminate into the bulk LC. Therefore, the ECE shows a strong frequency behavior and decreases significantly above 10^3 Hz—which makes it a surface-induced chirality phenomenon.

Acknowledgments: This work was supported by the Office of Naval Research (N0001420WX01656; N0001420WX01630; N0001420WX01703). The author would like to thank Prof. Charles Rosenblatt for useful discussions.

Figure captions

Figure 1: (a) Chemical structure and cooling phase sequence of LC 9004. (b) A schematic representation of graphene-PI cell. (c) A picture of the graphene-PI cell. (d) A micrograph of the Sm-*A* phase of 9004 in the graphene-PI cell where the LC director is at 45° with respect to the crossed polarizers. (e) A micrograph of the Sm-*A* phase of 9004 in the graphene-PI cell where the LC director is parallel to the polarizer and perpendicular to the analyzer. (f) A schematic representation of a strained graphene film. The Ph-O bond of the LC 9004 is twisted on the strained graphene film to maintain the π - π electron stacking interaction.

Figure 2: Electroclinic effect in the Sm-*A* phase: (a) the effective tilt angle θ vs. E ($f = 100$ Hz) for 9004 in the standard commercial uniform planar cell at two different values of T , listed in the legend, (b) the effective tilt angle θ vs. E ($f = 100$ Hz) for 9004 in the graphene-PI cell at three different values of T listed in the legend. Dotted lines represent linear fits.

Figure 3: (a) The electroclinic coefficient e_c vs. T showing pretransitional behavior. (b) The inverse of the electroclinic coefficient e_c^{-1} vs. T . A linear fit is shown near T_{AC^*} ($= 62$ °C).

Figure 4: The electroclinic coefficient e_c vs. f showing the relaxation dynamics of the ECE at $T = 63$ °C.

Reference

- [1] R. Basu, K. Boccuzzi, S. Ferjani and C. Rosenblatt; “Carbon nanotube induced chirality in an achiral liquid crystal,” *Appl. Phys. Lett.* **97**(12), 121908 (2010).
- [2] R. Basu, R.G. Petschek and C. Rosenblatt, “Nematic electroclinic effect in a carbon nanotube doped achiral liquid crystal,” *Phys. Rev. E* **83**(4), 041707 (2011).
- [3] P. Kalakonda, R. Basu, I.R. Nemitz, C. Rosenblatt, and G. S. Iannacchione, “Studies of nanocomposites of carbon nanotubes and a negative dielectric anisotropy liquid crystal,” *J. Chem. Phys* **140**(10), 104908 (2014).
- [4] R. Basu, C.-L. Chen, and C. Rosenblatt, “Carbon nanotube-induced macroscopic helical twist in an achiral nematic liquid crystal,” *J. Appl. Phys.* **109**(8), 083518 (2011).
- [5] R. Basu, C. Rosenblatt, and R. Lemieux; “Chiral induction in thioester and oxoester liquid crystals by dispersed carbon nanotubes,” *Liq. Cryst.* **39**(2), 199 (2012).
- [6] V. Jayalakshmi, T. Wood, R. Basu, J. Du, T. Blackburn, C. Rosenblatt, C. M. Crudden, and R. P. Lemieux, “Probing the pore structure of a chiral periodic mesoporous organosilica using liquid crystals,” *J. Mater. Chem.* **22**(30), 15255-15261 (2012).
- [7] I.R. Nemitz, K. McEleney, C.M. Crudden, R.P. Lemieux, R.G. Petschek and C. Rosenblatt, “Chiral periodic mesoporous organosilica in a smectic-A liquid crystal: source of the electrooptic response,” *Liquid Crystals* **43**(4), 497-504 (2016).
- [8] R. Basu, J.S. Pendery, R.G. Petschek, R.P. Lemieux, and C. Rosenblatt, “Macroscopic Torsional Strain and Induced Molecular Conformational Deracemization,” *Phys. Rev. Lett.* **107**(23), 237804 (2011).
- [9] R. Basu, I.R. Nemitz, Q. Song, R. P. Lemieux, and C. Rosenblatt, “Surface topography and rotational symmetry breaking,” *Phys. Rev. E* **86**(1), 011711 (2012).
- [10] T.-C. Lin, I.R. Nemitz, J.S. Pendery, C.P.J. Schubert, R.P. Lemieux, and C. Rosenblatt, “Nematic twist cell: Strong chirality induced at the surfaces,” *Appl. Phys. Lett.* **102**(13), 134101 (2013).
- [11] S. Ferjani, Y. Choi, J. Pendery, R.G. Petschek, and C. Rosenblatt, “Mechanically Generated Surface Chirality at the Nanoscale,” *Phys. Rev. Lett.* **104**(25), 257801 (2010).
- [12] S. Ferjani, J. Pendery, and C. Rosenblatt, “Mechanically generated surface chirality: Control of chiral strength”, *Appl. Phys. Lett.* **97**(12), 121905 (2010).

-
- [13] J. Pendery, S. Ferjani, C. Rosenblatt, and R.G. Petschek, “Spatially controllable surface chirality at the nanoscale,” *Europhysics Letters* **96**(2), 26001 (2011).
- [14] F. Charra and J. Cousty, “Surface-Induced Chirality in a Self-Assembled Monolayer of Discotic Liquid Crystal,” *Phys. Rev. Lett.* **80**(8), 1682 (1998).
- [15] S. Garoff and R.B. Meyer, “Electroclinic Effect at the A–C Phase Change in a Chiral Smectic Liquid Crystal,” *Phys. Rev. Lett.* **38**(15), 848 (1977).
- [16] D.W. Kim, Y.H. Kim, H.S. Jeong, and H.-T. Jung, “Direct visualization of large-area graphene domains and boundaries by optical birefringency,” *Nat. Nanotechnol.* **7**(1), 29-34 (2012).
- [17] M.A. Shehzad, D.H. Tien, M.W. Iqbal, J. Eom, J.H. Park, C. Hwang, and Y. Seo, “Nematic liquid crystal on a two dimensional hexagonal lattice and its application,” *Sci. Rep.* **5**, 13331 (2015).
- [18] J. S. Yu, D.H. Ha, and J. H. Kim, “Mapping of the atomic lattice orientation of a graphite flake using macroscopic liquid crystal texture”, *Nanotechnology* **23**(39), 395704 (2012).
- [19] M.A. Shehzad, S. Hussain, J. Lee, J. Jung, N. Lee, G. Kim, and Y. Seo, “Study of Grains and Boundaries of Molybdenum Diselenide and Tungsten Diselenide Using Liquid Crystal,” *Nano Lett.* **17**(3), 1474–1481 (2017).
- [20] D.W. Kim, J.M. Ok, W.-B. Jung, J.-S. Kim, S. J. Kim, H.O. Choi, Y.H. Kim, H.-T. Jung, “Direct Observation of Molybdenum Disulfide, MoS₂, Domains by Using a Liquid Crystalline Texture Method,” *Nano Lett.* **15**(1), 229-234 (2015).
- [21] R. Basu, L.J. Atwood, “Two-dimensional hexagonal boron nitride nanosheet as the planar-alignment agent in a liquid crystal-based electro-optic device,” *Opt. Express* **27**(1), 282-292 (2019).
- [22] R. Basu and L. Atwood, “Electro-optic liquid crystal device employing two-dimensional WSe₂ as the planar-alignment layers”, *Opt. Mater. Express* **10**(6), 1405-1412 (2020).
- [23] Y.J. Lim, B.H. Lee, Y.R. Kwon, Y.E. Choi, G. Murali, J.H. Lee, V.L. Nguyen, Y.H. Lee, and S.H. Lee, “Monitoring defects on monolayer graphene using nematic liquid crystals,” *Opt. Express* **23**(11), 14162-14167 (2015).
- [24] R. Basu and S.A. Shalov, “Graphene as transmissive electrodes and aligning layers for liquid-crystal-based electro-optic devices,” *Phys. Rev. E* **96**(1), 012702 (2017).
- [25] R. Basu and A. Lee, “Ion trapping by the graphene electrode in a graphene-ITO hybrid liquid crystal cell,” *Appl. Phys. Lett.* **111**(16), 161905 (2017).

-
- [26] R. Basu and L.J. Atwood, “Characterizations of a Graphene-Polyimide Hybrid Electro-optical Liquid Crystal Device,” *OSA Continuum* **2**(1), 83-91 (2019).
- [27] T. Jiang, D. Emerson, K. Twarowski, D. Finkenstadt, J. Therrien, “Rotation of the linear-polarization plane of transmitted and reflected light by single- and few-layer graphene,” *Phys. Rev. B* **82**(23), 235430 (2010).
- [28] R. Basu, D. Kinnamon, and A. Garvey, “Detection of graphene chirality using achiral liquid crystalline platforms,” *J. Appl. Phys.* **118**(11), 114302 (2015).
- [29] R. Basu, D. Kinnamon, and A. Garvey, “Graphene and liquid crystal mediated interactions,” *Liquid Crystals* **43**(13-15), 2375-2390 (2016).
- [30] I.R. Nemitz, I. Gryn, N. Boudet, R.P. Lemieux, M. Goldmann, B. Zappone, R.G. Petschek, C. Rosenblatt, E. Lacaze, “Observations of a streak texture in the hybrid-aligned smectic-C phase,” *Soft Matter* **14**(3), 460-469 (2018).
- [31] X. Li, Y. Zhu, W. Cai, M. Borysiak, B. Han, D. Chen, R. D. Piner, L. Colombo, and R. S. Ruoff, “Transfer of Large-Area Graphene Films for High-Performance Transparent Conductive Electrodes,” *Nano Lett.* **9**(12), 4359–4363 (2009).
- [32] X. Liang, B.A. Sperling, I. Calizo, G. Cheng, C. A. Hacker, Q. Zhang, Y. Obeng, K. Yan, H. Peng, Q. Li, X. Zhu, H. Yuan, A.R.H. Walker, Z. Liu, L.-M. Peng, and C.A. Richter, “Toward clean and crackless transfer of graphene,” *ACS Nano* **5**(11), 9144–9153 (2011).
- [33] Z. Yan, J. Lin, Z. Peng, Z. Sun, Y. Zhu, L. Li, C. Xiang, E.L. Samuel, C. Kittrell, and J.M. Tour, “Toward the Synthesis of Wafer-Scale Single-Crystal Graphene on Copper Foils,” *ACS Nano* **6**(10), 9110-9117 (2012).
- [34] G. Andersson, I. Dahl, P. Keller, W. Kuczynski, S.T. Lagerwall, K. Skarp, and B. Stebler, “Submicrosecond electro-optic switching in the liquid-crystal smectic A phase: The soft-mode ferroelectric effect,” *Appl. Phys. Lett.* **51**(9), 640 (1987).
- [35] Z. Li, R.G. Petschek, and C. Rosenblatt, “Linear Electroclinic Effect in a Chiral Nematic Liquid Crystal,” *Phys. Rev. Lett.* **62**(7), 796 (1989).
- [36] R. Qiu, J.T. Ho, and S.K. Hark, “Electroclinic effect above the smectic-A-smectic-C transition,” *Phys. Rev. A* **38**(3), 1653-1655 (1988).
- [37] Z. Li and C. Rosenblatt, “Origin of the anomalous electroclinic susceptibility exponent in a ferroelectric liquid crystal,” *Phys. Rev. A* **39**(3), 1594-1596 (1989).
- [38] S.T. Lagerwall, *Ferroelectric and Antiferroelectric Liquid Crystals* (Wiley-VCH, Weinheim, Germany, 1999).

-
- [39] Phil Szuromi, “Strained Graphene,” *Science* **325**(5940), 518 (2009).
- [40] G. Andersson, I. Dahl, L. Komitov, S.T. Lagerwall, K. Skarp, and B. Stebler, “Device physics of the soft \square mode electro \square optic effect,” *Journal of Applied Physics* **66**(10), 4983 (1989).
- [41] S.T. Lagerwall, M. Matuszczyk, P. Rodhe, L. Odman, “*The Electroclinic Effect*,” in S. J. Elston, J. R. Sambles (eds) *The Optics of Thermotropic Liquid Crystals* (Taylor & Francis, London, 1998).
- [42] C.L. Folcia, J. Ortega, and J. Etxebarria, “Electroclinic effect around a smectic A-chiral nematic phase transition,” *Liquid Crystals* **29**(6), 765-773 (2002).
- [43] M.H. Zhu, G. Carbone, and C. Rosenblatt, “Quasi divergent nematic surface electroclinic effect,” *Phys. Rev. E* **73**(4), 041701 (2006).

Fig. 1

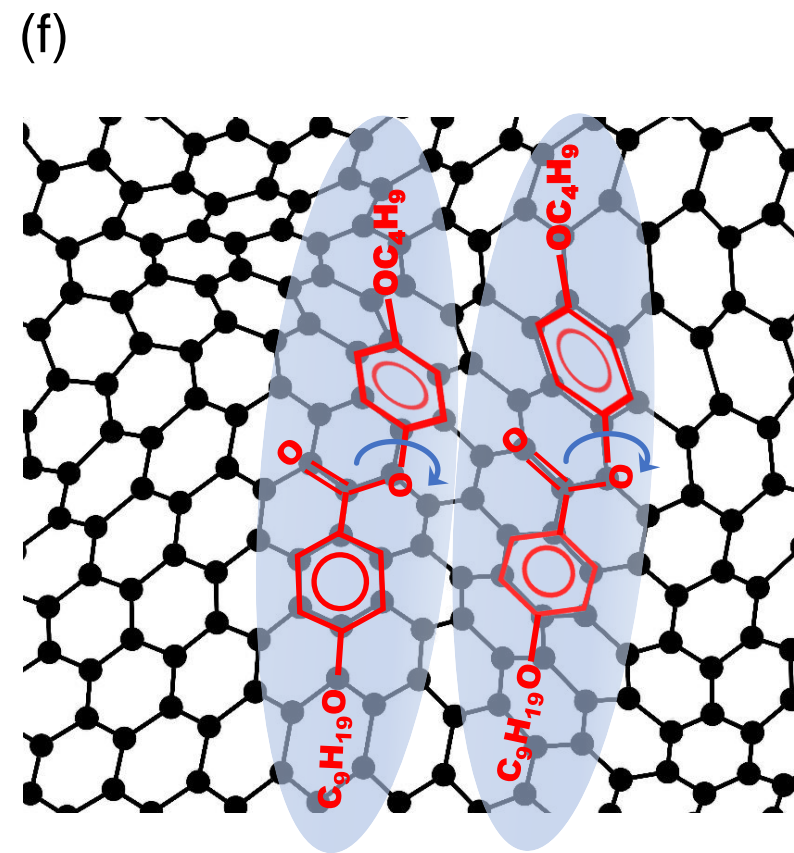
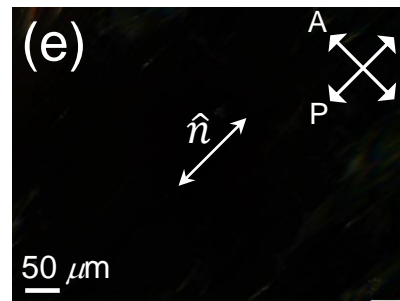
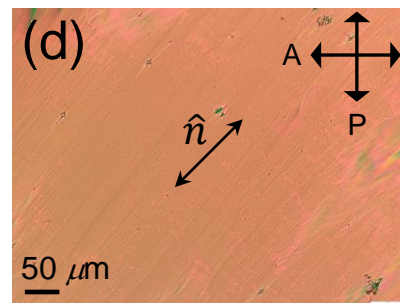
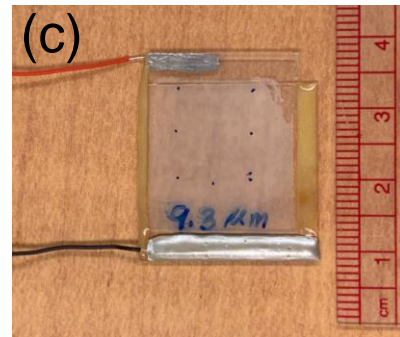
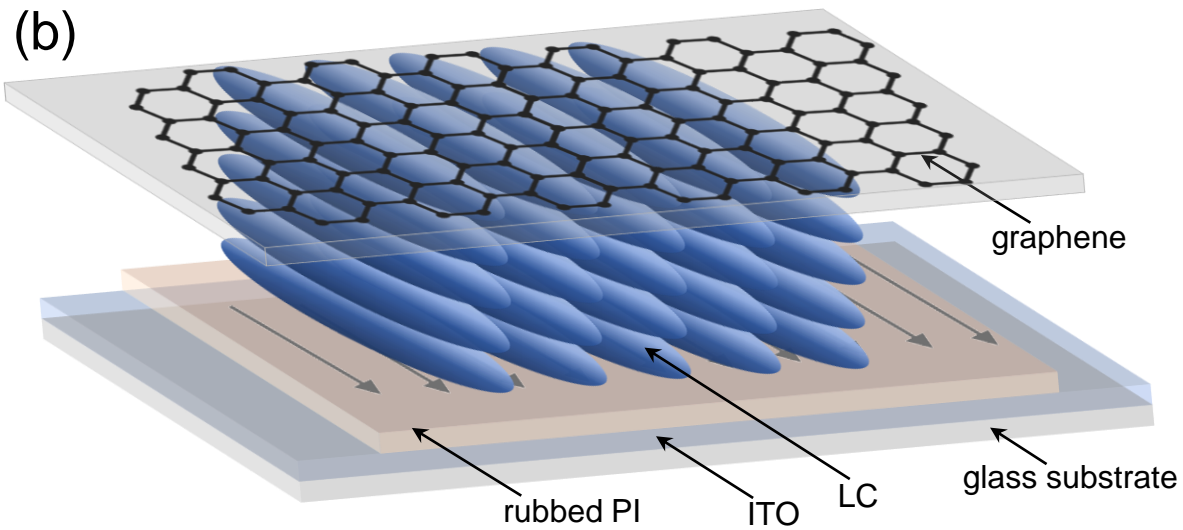
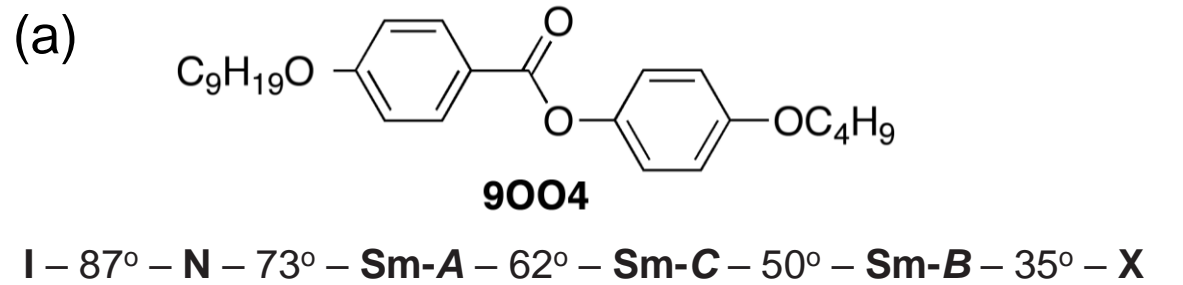


Fig. 2

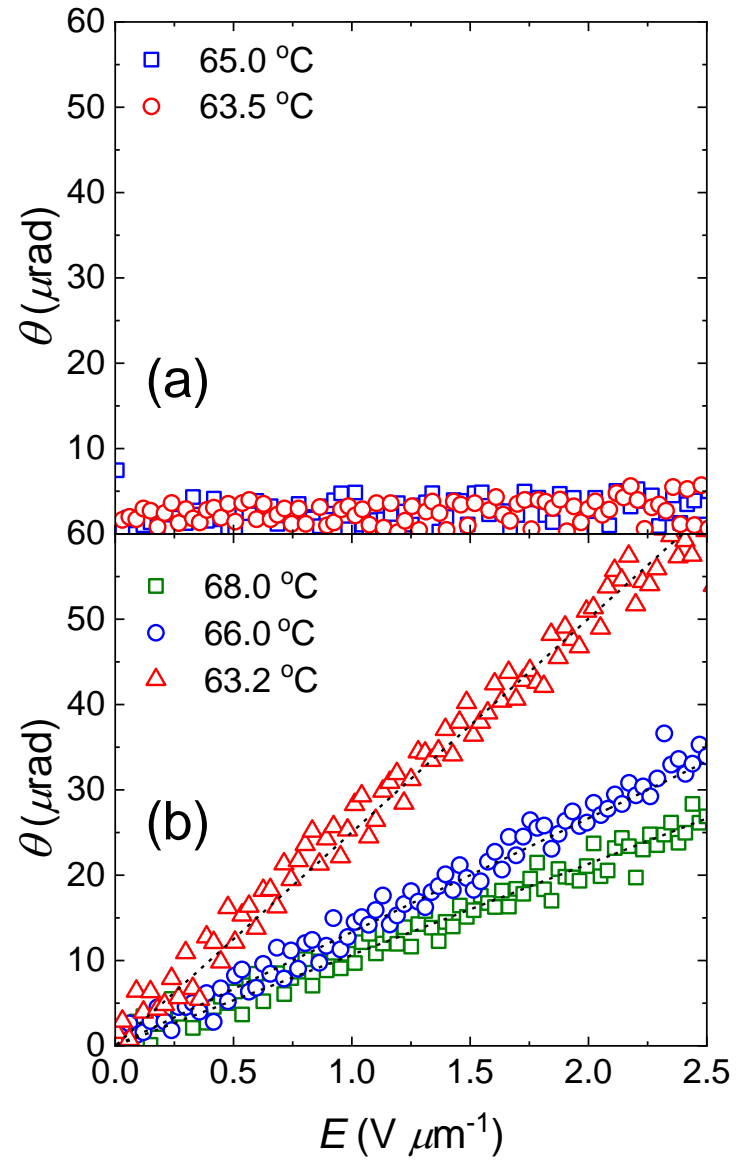


Fig. 3

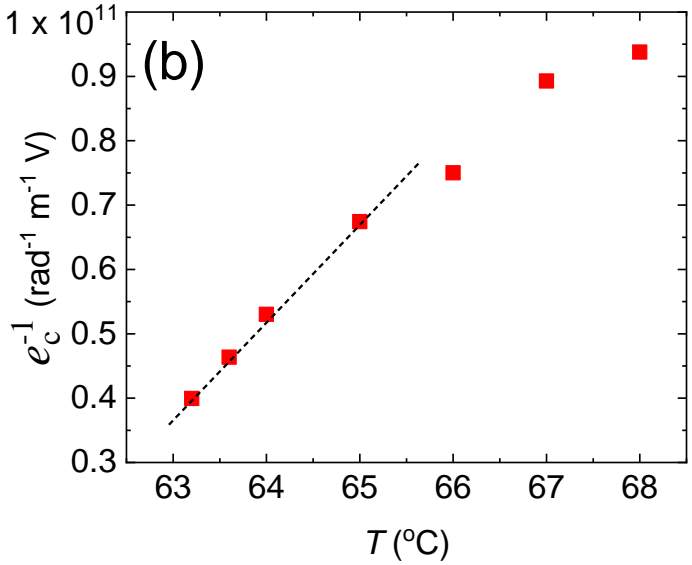
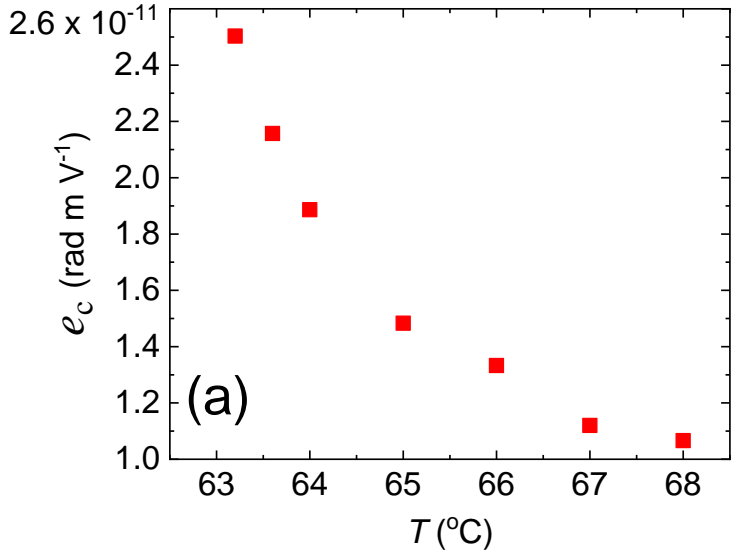


Fig. 4

